International Journal of Industrial and Manufacturing Systems Engineering
2023; 8(2): 30-41
http://www.sciencepublishinggroup.com/j/ijimse
doi: 10.11648/j.ijimse.20230802.12
ISSN: 2575-3150 (Print); ISSN: 2575-3142 (Online)

Research on the Online Monitoring of the Service Status of Hot-Rolling Mill Work Rolls and Online Decision-Making Method for Active Remanufacturing

Yuhao Zhang, Chen Wei, Xiaoqing Tian*, Shouxu Song

School of Mechanical Engineering, Hefei University of Technology, Hefei, China

Email address:

zhang_yhao@163.com (Yuhao Zhang), 2017110197@mail.hfut.edu.cn (Chen Wei), tianxiaoqing@hfut.edu.cn (Xiaoqing Tian)

*Corresponding author

To cite this article:

Yuhao Zhang, Chen Wei, Xiaoqing Tian, Shouxu Song. Research on the Online Monitoring of the Service Status of Hot-Rolling Mill Work Rolls and Online Decision-Making Method for Active Remanufacturing. *International Journal of Industrial and Manufacturing Systems Engineering*. Vol. 8, No. 2, 2023, pp. 30-41. doi: 10.11648/j.ijimse.20230802.12

Received: October 25, 2023; **Accepted**: November 9, 2023; **Published**: November 17, 2023

Abstract: The remanufacturing of rolling mill rolls offers significant economic, environmental, and societal benefits. However, the uncertainty surrounding the performance degradation of retired rolls and its associated timeline poses challenges to the efficiency and cost-effectiveness of roll remanufacturing operations. Therefore, the real-time monitoring of the degradation status of rolling mill rolls is of paramount importance. This study presents an approach that combines multi-sensor data fusion with a multilayer perceptron (MLP) model, which takes into account economic considerations to predict the degradation status of hot-rolling mill work rolls and make online decisions for active remanufacturing. The degradation process of rolling mill rolls is analyzed, and degradation performance indicators are established. Eddy current signals and torque signals from the rolling mill surface are collected during the roll degradation experiments. The friction coefficient and energy of the Hilbert spectrum of the eddy current signal are used as online input features for the MLP model, which is trained using the degradation experiment data. The superiority of the proposed MLP model is validated through rolling mill roll degradation experiments. Based on the predictions of the MLP model, the optimal timing for remanufacturing rolling mill rolls in the time domain is evaluated using Wiener and update-reward theories. This approach enables the online monitoring and quantitative characterization of the comprehensive degradation of high-speed steel work rolls and facilitates online decision-making regarding the optimal timing for active remanufacturing.

Keywords: Hot Rolling Mill Rolls, Active Remanufacturing, Online Monitoring, Machine Learning

1. Introduction

Rolling is a highly popular metal-forming process, and rolling mill rolls are among the most critical components in rolling operations [1]. During rolling, hot-rolling rolls come into contact with the high-temperature workpiece, where the roll surface temperature exceeds 500°C [2, 3]. Simultaneously, the rolls need cooling fluid to cool their surfaces. They are subjected to prolonged exposure to high-temperature, high-stress, and humidity conditions. Consequently, the roll surfaces undergo oxidation, and alloy carbides and carbon precipitation decompose, which degrades the roll surface properties, e.g., the hardness, wear resistance, and resistance to heat cracking decrease. Since the condition of the work roll surfaces directly affects the profile of the rolled steel, the product quality is significantly affected. Moreover, the condition of the work roll surfaces is closely related to roll fatigue [4]. Therefore, it is essential to monitor the operational status of the rolls. Furthermore, after the rolls have been retired, the failed portion accounts for only 10–15% of the entire roll and is primarily concentrated on the roll surface. To fully use the core of the roll and some non-failed layers, it is necessary to re-manufacture the rolls. Roll remanufacturing offers excellent economic, environmental, and societal benefits. However, due to the variations in the time and condition of the roll retirement, there is uncertainty in the quality of re-manufactured rolls, which can impede the progress of remanufacturing efforts. Thus, real-time

assessment of the roll conditions is required. The real-time assessment of the roll conditions is a crucial aspect of addressing the uncertainty in roll remanufacturing and plays a vital role in efficiently advancing and managing roll remanufacturing operations.

WEIDLICH et al. [5] proposed a surface damage coefficient (k) to assess the surface thermal damage and plastic strain of rolls by integrating three process parameters with weighting. When k exceeds 375, thermal fatigue dominates the damage. WU et al. [6] introduced a time-varying oil film stiffness model to identify the size of surface defects on rolls. LI et al. [7] used finite element methods to demonstrate that the surface stress differences on rolls could reach 145.7 MPa, and excessive stress differences accelerated the roll fatigue. GARZA-MONTES-DE-OCA et al. [8] simulated thermal fatigue in high-speed steel rolling rolls through roll testing during thermal cycling, which led to roll oxidation, carbide decomposition, and peeling in high-frequency thermal cycling. XU et al. [9] noted that the slip ratio determined the wear failure mode, which affected the wear performance of high-speed steel rolling rolls. When the slip ratio reaches 5.5%, the friction coefficient on the roll surface reaches its peak.

Traditional analysis methods focus on the micro-mechanical aspects of the working process roll conditions, but the subsequent operational status of rolls remains uncertain. DENG et al. [10] conducted research on the temperature and stress fields to simulate the temperature changes of rolls and assess their oxidation behavior. They noted that the location of carbide spalling was often where cracks were initiated [11]. SUN et al. [12] proposed a comprehensive finite element-based model to predict the steady-state thermodynamic behavior of the strip-roll system and the lifespan of the roll. Therefore, they introduced a roll active remanufacturing design approach that considers the relationships among multiple rolls.

Previous research often focused on examining only one specific aspect of roll degradation. However, the failure of rolls is influenced by multiple factors and cannot be determined by a single indicator [7]. Relying on a single evaluation metric may result in an incomplete assessment of the roll condition. Therefore, there is a need for a comprehensive and real-time method to assess the roll status. The selection of an appropriate timing for roll remanufacturing is also a critical aspect of roll remanufacturing efforts. However, research on the decision-making process regarding the timing of roll remanufacturing is scarce. Gan et al. proposed a digital twin model based mold wear monitoring method to improve the part quality during stamping [13]. Moreover, they developed a IoT based energy efficiency monitoring method to reduce the energy consumption in stamping workshop, which improves economic efficiency [14]. So, the decision regarding the timing of roll remanufacturing should inherently consider the economic benefits. In other words, the technical condition of the rolls and the costs and benefits associated with remanufacturing should be considered to make the most suitable decision. Research on this issue is of paramount importance for the efficient management and economic efficiency of roll remanufacturing work.

To address the aforementioned challenges in roll remanufacturing, this study proposes an online method that combines multi-sensor data with multiple features and a multilayer perceptron (MLP) model considering the economic benefits. This approach aims to predict the degradation status of hot-rolling mill work rolls and make active remanufacturing decisions in real time. Based on roll degradation experiments, the study analyzes roll degradation and constructs a comprehensive roll health indicator using the Beta method. This indicator quantitatively characterizes the health status of the rolls. An MLP model is established to predict the roll performance degradation using online monitoring methods. By combining online monitoring techniques, the friction coefficient during the roll degradation process is computed, and time-frequency spectral energy sum features are extracted from pulse eddy current signals. These online features serve as input vectors for the MLP model to enable the real-time monitoring and prediction of the roll degradation status. Finally, using the update-reward theory, this study provides optimal remanufacturing timing points for the rolls considering the economic benefits. This work advances the monitoring of the real-time roll status and identification of the optimal active remanufacturing timing.

2. Proposed Method

The study introduces an online method to predict the degradation status of hot-rolling mill work rolls and make active remanufacturing decisions while considering the economic benefits. Figure 1 illustrates the overall process flowchart. The process of predicting the degradation status and making active remanufacturing decisions for hot-rolling mill work rolls online mainly includes the characterization of the roll degradation status, selection and extraction of online features, design and training of the MLP model, and economic evaluation. The training of the MLP model relies on signals collected during equivalent simulated experiments that involve the rolling mill, and the degradation status of the rolls is evaluated based on a combination of multiple indicators. To monitor the rolls online, inputs that can be obtained online are extracted and used as inputs for the MLP model. Furthermore, before training the MLP model, considering the variability of signals from multiple sources, the features extracted from multiple sensors are normalized to reduce the computational complexity and enhance the model accuracy. Iterative training yields an MLP model with high accuracy in recognizing the degradation status of the rolls. Based on the remanufacturing timing provided by the MLP model, the optimal timing for roll remanufacturing in the time domain is evaluated using the update-reward theory.

2.1. Roller Degradation State Representation

During the rolling process, hot-rolling mill rolls come into contact with the high-temperature workpiece, where the roll

surface temperature in the contact zone exceeds 500°C [2]. Simultaneously, the rolls require a cooling fluid to cool their surfaces. Being exposed to prolonged high-temperature, high-stress, and humid conditions, the roll surface oxidizes over time. This oxidation decomposes the alloy carbides and carbon precipitation, which degrades the roll surface properties such as the hardness, wear resistance, and resistance to thermal cracking. Changes in hardness can alter the friction coefficient between the work roll and the workpiece, where lower hardness corresponds to lower wear resistance and more severe wear [15]. The decline in surface hardness of the rolls during their service life can reduce the quality of rolled products and exacerbate roll surface deterioration and wear.

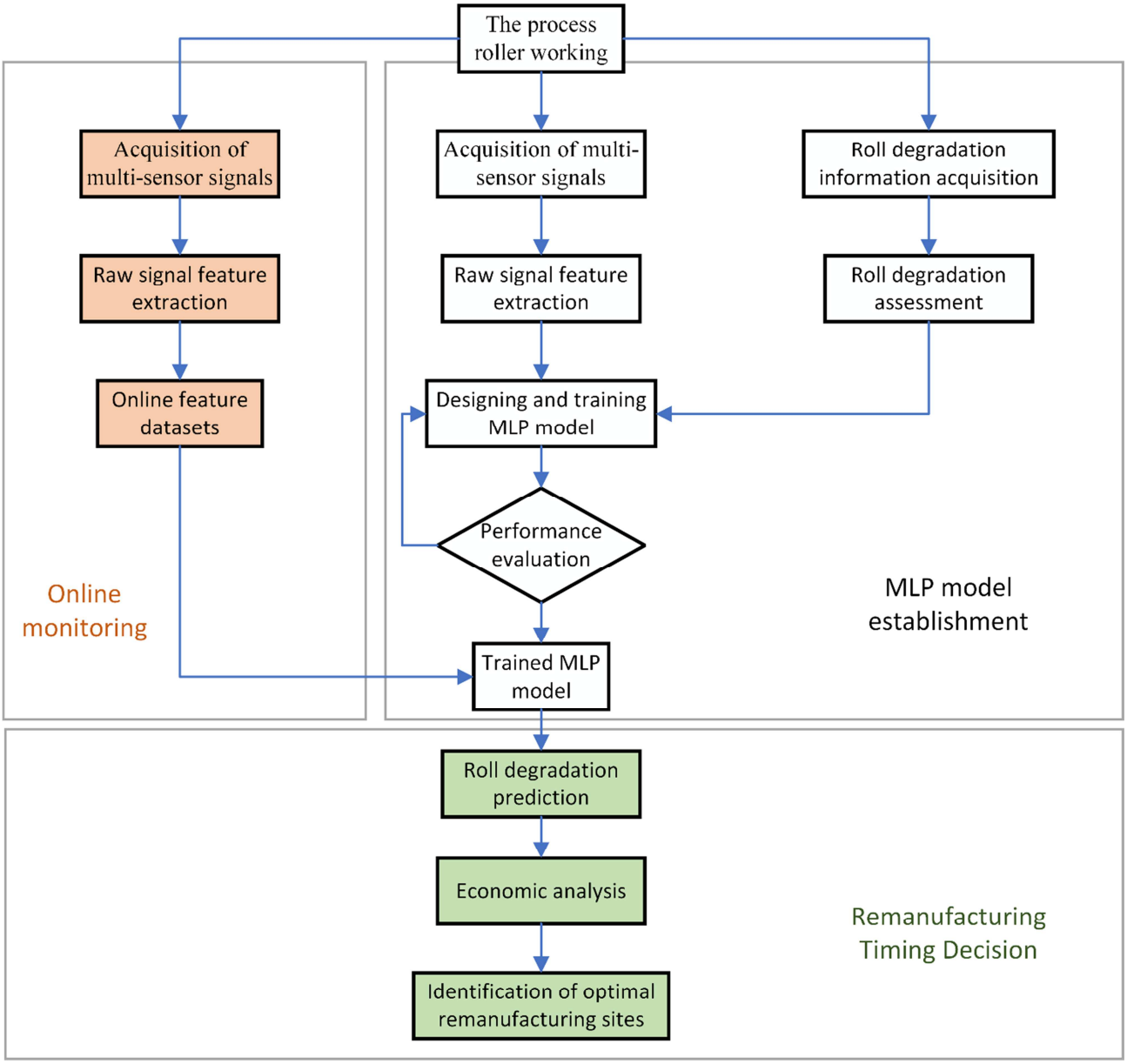

Figure 1. *Flowchart of the roll work status prediction and remanufacturing timing decision.*

Roll wear is a primary contributor to the shortened lifespan of rolls [15], where cumulative wear accumulates through various stages of wear.

$$M_i = \sum_{n=1}^{i} m_i \tag{1}$$

In the equation, M_i is the cumulative wear amount for the i-th cycle, and m_i is the stage wear amount.

In summary, since oxidation and cracks cannot be quantitatively described, to comprehensively characterize the working condition of rolls during service, the roll hardness, wear amount, and wear resistance (stage wear amount) are ultimately selected as the assessment of roll degradation. Different indicators of the rolls degrade at varying rates during their use, such as [insert example]. Therefore, to determine the optimal point for the comprehensive performance indicator of rolls, it is necessary to comprehensively evaluate various

degradation indicators.

The Beta distribution measures the likelihood of all possible probabilities and can be considered the probability distribution function for each probability. In each cycle of rolling mill operation, each assessment indicator can be represented by a Beta distribution. After various assessment indicators have been standardized, they share the same range of values as the Beta distribution. Therefore, the Beta distribution can flexibly represent various probability distribution functions. In this study, based on the Beta distribution, the set of roll status assessment indicators is fused to comprehensively represent the health status of a roll. The process of characterizing the roll health status based on the Beta distribution is as follows:

Step1: Building and Normalization of the Evaluation Index Matrix

$$A=\begin{bmatrix} x_{11} & x_{12} & \cdots & x_{1n} \\ x_{21} & x_{22} & \cdots & x_{2n} \\ \vdots & \vdots & & \vdots \\ x_{m1} & x_{m2} & \cdots & x_{mn} \end{bmatrix} (i=1,2,...,m; j=1,2,...,n) \quad (2)$$

Here, i is the number of stage states that correspond to the rolls, j is the number of degradation indicators in the assessment indicator set, and x_{ij} is the value of the j-th assessment indicator of the roll in the i-th stage state.

To eliminate the influence of different orders of magnitude and dimensions among different degradation indicators, it is necessary to normalize the indicator matrix. Common normalization methods include linear normalization, nonlinear normalization, and standardization. Regarding roll degradation indicators, the trends of various degradation indicators slowly change, the values are relatively concentrated, and the maximum and minimum values of each indicator remain relatively stable during the roll degradation process. Therefore, this study chooses the linear normalization method.

The indicators are further classified into positive and negative indicators. In this context, the performance of the rolls is positively correlated with the hardness and wear resistance and negatively correlated with the wear amount and surface rough-ness. In other words, the hardness and wear resistance are positive indicators, while the wear amount is a negative indicator as follows:

$$positive\ indicator: b_{ij}=\frac{a_{ij}-\min(a_j)}{\max(a_j)-\min(a_j)} \quad (3)$$

$$negative\ indicator: b_{ij}=\frac{\max(a_j)-a_{ij}}{\max(a_j)-\min(a_j)} \quad (4)$$

where b_{ij} is the normalized value that corresponds to the j-th assessment indicator of the roll in the i-th stage state.

Step2: Indicator Fusion

The Beta distribution is used to combine the normalized and weighted indicators of the roll hardness, wear amount, and wear resistance. The probability density function (PDF) form of the Beta distribution is as follows:

$$f(x;\alpha,\gamma)=\frac{x^{\alpha-1}(1-x)^{\gamma-1}}{\int_0^1 u^{\alpha-1}(1-u)^{\gamma-1}du}, 0<x<1, \alpha>0, \gamma>0 \quad (5)$$

The PDF that corresponds to the roller state at cycle k is given by the following equation, where α and β are the shape parameters of the Beta distribution:

$$f_k(x_k;\alpha_k,\gamma_k)=\frac{x_k^{\alpha_k-1}(1-x_k)^{\gamma_k-1}}{\int_0^1 u^{\alpha_k-1}(1-u)^{\gamma_k-1}} \quad (6)$$

The estimated values of parameters α_k and γ_k are:

$$\alpha_k=\sum_{j=1}^{n} w_{jk}b_{jk} \quad (7)$$

$$\gamma_k=\sum_{j=1}^{n} w_{jk}\left(1-b_{jk}\right) \quad (8)$$

$$\gamma_k=\sum_{j=1}^{n} w_{jk}\left(1-b_{jk}\right) \quad (9)$$

In the equation, $b_{jk}\ (j=1,2,...,n)$ is the normalized values of various indicators for cycle k, and w_{jk} is the weight of indicator b_{jk}. The weights are evenly distributed, and the point estimate of the roller's state indicators HI_k for each cycle is calculated using the maximum likelihood.

2.2. Acquisition and Processing of Online Features

2.2.1. Selection of Online Monitoring Methods

To monitor the rolls online, the selected detection method should be capable of operating while the rolling mill is in operation. Xu et al. propose a classification model with multi-sensor inputs, and the results show that the introduction of multiple sensors significantly improves the classification accuracy of the model compared to a single sensor based model [16]. Therefore, this study uses multiple sensors as model inputs. Common online monitoring methods include electromagnetic testing, ultrasonic testing, radiographic testing, and machine vision inspection. Among these methods, radiographic testing is typically suitable for detecting defects such as cracks in static structures. Due to its high penetration depth and requirement for coupling agents, ultrasonic testing is more suitable for detecting internal defects in objects and challenging for monitoring rolls in active service [12]. Pulse eddy current testing is an improved version of the traditional eddy current testing, which follows Faraday's electromagnetic induction law. Its principle involves using a pulse eddy current probe to induce an excitation magnetic field (i.e., a primary

field) without requiring contact with the test object. This induction is achieved through pulsed excitation with certain frequency, amplitude, and duty cycle values and results in vortex-like pulsed currents on the sur-face of the test object. These generated eddy currents induce a detection-induced magnetic field (i.e., a secondary field) and couple with the primary field to form a compo-site coupling magnetic field. The coupling magnetic field is an alternating field with attenuation characteristics. During the operation of hot-rolling work rolls, the martensitic matrix underwent magnetic softening, which increased the magnetic permeability and decreased the coercivity. Therefore, roll degradation can affect the coupling magnetic field, and its degradation information can be detected in the pulse eddy current signal. Furthermore, for finishing stands in rolling mills, a low friction coefficient is a critical factor in roll selection. Increased wear also causes an increase in adhesive defects [17]. Bataille et al. [18] noted that the surface friction coefficient directly affected the surface of the rolled steel plate, and an increase in friction coefficient increased the rolling force [15]. The friction coefficient can be calculated from the torque, which can be obtained using sensors.

In conclusion, in this study, we use pulse eddy current sensors and torque sensors to monitor rolls online.

2.2.2. Online Monitoring Signal Processing

The friction coefficient is calculated from the torque obtained using the torque sensor as follows:

$$f = \frac{T}{rF} \tag{10}$$

where r is the roll radius, F is the rolling force, and T is the torque generated during the operation of the work roll.

Processing pulse eddy current signals requires selecting an appropriate processing method. The Hilbert-Huang transform (HHT) is a novel time-frequency analysis method suitable for handling complex non-stationary signals. Traditional HHT begins with an empirical mode decomposition (EMD) of the original signal, which divides it into several intrinsic mode functions (IMFs). Subsequently, Hilbert transformation is applied. This method offers complete adaptability and is not constrained by the uncertainty principle. It simultaneously provides high time resolution and high frequency resolution. However, the IMFs obtained through EMD can sometimes exhibit similar frequency components, which results in mode mixing. This issue can be effectively ad-dressed by replacing the EMD with variational mode decomposition (VMD). In VMD, a variational problem is constructed to seek the optimal solution to determine the center frequency and bandwidth of each IMF. Therefore, in this study, the VMD-Hilbert transformation method is used to decompose pulse eddy current signals. This method constructs a variational problem to find the optimal solution for the center frequency and bandwidth of each IMF. Hilbert spectral energy is extracted from the pulse eddy current signals as an online feature.

The Hilbert spectral energy obtained using the VMD-Hilbert method is represent-ed as follows:

$$H(w,t) = \mathrm{Re}\sum_{i=1}^{n} A_i(t)e^{-i\int \omega_i(t)\mathrm{d}t} \tag{11}$$

$$E = \int_0^{\infty}\int_0^{\infty} H(w,t)\mathrm{d}t\mathrm{d}\omega \tag{12}$$

$$\omega_i(t) = 2\pi \mathrm{f}_i = \frac{\mathrm{d}\varphi_i(t)}{\mathrm{d}t} \tag{13}$$

In the equation, $H(w,t)$ is the Hilbert spectrum obtained after applying the VMD-Hilbert transformation to the original signal, and E is the Hilbert spectral energy.

2.3. Model Design and Training

2.3.1. Model Design

The design of the MLP model is of crucial significance for uncovering the complex intrinsic relationships and underlying patterns between multiple features and roll degradation. Given its strong data mining and feature extraction capabilities, this study presents a hot-rolling roll degradation prediction model based on MLP. This model is used to monitor the roll degradation online during the rolling process.

To minimize the influence of sample errors on the accuracy of the MLP model, in this study, we extract the online monitoring features from eight different points on the roll for each rolling cycle as the input to the MLP model. The hidden layer is a crucial component of the MLP model. When training the MLP model to predict the roll degradation status, the number of hidden layers and neurons in the hidden layers must be optimized and adjusted. The prediction accuracy of roll degradation increases with an increase in the number of hidden layers and neurons, but too many neurons and hid-den layers during the MLP model training can cause overfitting problems. Meanwhile, if there are too few parameters in the hidden layers, the model may not achieve the de-sired accuracy during training. Therefore, to strike a balance between the training time and the accuracy of the roll degradation prediction, it is necessary to select appropriate hidden layer parameters based on experimentation.

The training process of the MLP model primarily consists of three components: First, multi-source online feature information from multiple sensors is extracted during the workpiece processing. These various source signals are used as the input matrix for the model to predict the roll degradation state that corresponds to the input data at that moment. Subsequently, it entails the computation of errors for all neurons during the back-propagation phase. Finally, based on these errors, the training process up-dates the gradient for each weight and subsequently adjusts the parameters of the MLP model. Through iterative training, the optimal online prediction model for roll degradation is achieved.

2.3.2. Model Evaluation Methods

To validate the feasibility and superiority of the proposed method for predicting roll degradation, two evaluation metrics were selected: mean absolute error (MAE) and mean absolute

percentage error (MAPE) [19]. The MAE and RMSE values exhibit a negative correlation with the prediction accuracy of roll degradation, which implies that smaller values of these evaluation metrics correspond to a higher predictive ac-curacy. The respective formulas for their calculation are as follows:

$$MAE = \frac{1}{m}\sum_{i=1}^{m} | \hat{y}_i - y_i | \tag{14}$$

$$RMSE = \sqrt{\frac{1}{m}\sum_{i=1}^{m} (\hat{y}_i - y_i)^2} \tag{15}$$

In the equations, "y_i" and "$\hat{y}_i$" are the actual and predicted values of roll degradation, respectively.

2.4. Considering Economic Factors in Remanufacturing Timing Decision

In theory, it is optimal to proactively re-manufacture the rolls at the inflection point of the roll performance indicators. However, in practical production processes, the situation is more complex, and factors such as the economic costs must often be considered with the roll performance. To determine the proactive remanufacturing timing domain, the economic optimal point can be selected within this domain and used as the proactive remanufacturing timing point for the rolls. Therefore, a comprehensive economic analysis of the rolls is required. The research objective of the proactive remanufacturing timing model for hot-rolling work rolls is to maximize their ser-vice life while ensuring that the expected cost rate remains low during their use and that the roll operation is stable.

The cost of scrapping and replacing hot-rolling work rolls can be expressed as follows:

$$c_{\mathrm{f}} = c_{\mathrm{n}} + c_{\mathrm{w}} + c_{\mathrm{h}} + c_{\mathrm{e}} + c_{\mathrm{t}} + c_{\mathrm{o}} \tag{16}$$

where c_f is the total cost of scrapping and replacing hot-rolling work rolls; c_n is the cost of purchasing new rolls; c_w is the expense of handling the old work rolls; c_h is the labor costs; c_e is the depreciation expenses related to equipment; c_t includes the inspection and evaluation costs; and c_o is the administrative and office management expenses.

The hot-rolling work roll remanufacturing process can be divided into three main parts: pre-treatment, laser cladding, and post-processing. Figure 2 illustrates the specific steps.

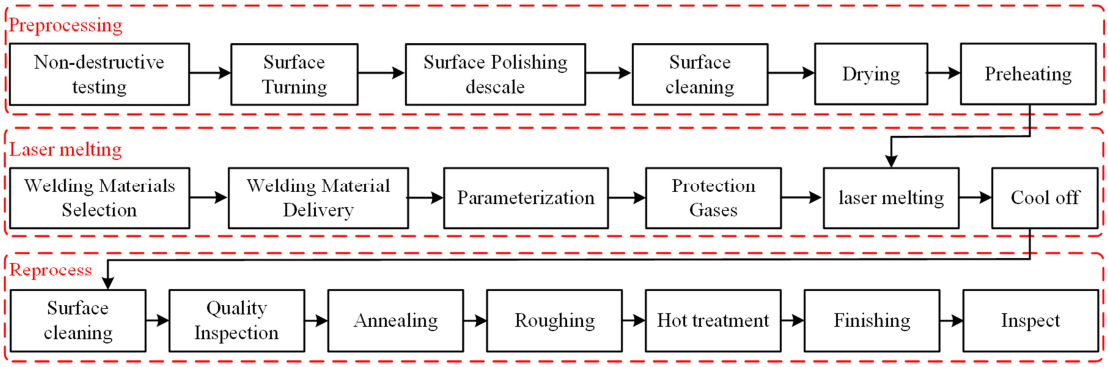

Figure 2. *Work roll remanufacturing process flow chart in hot rolling.*

In addition, the entire remanufacturing process must consider the costs associated with disassembly, commissioning, and labor. Taking into account all of these factors, the cost of hot-rolling work roll proactive remanufacturing is as follows:

$$c_{\mathrm{p}} = c_{\mathrm{l}} + c_{\mathrm{c}} + c_{\mathrm{a}} + c_{\mathrm{d}} + c_{\mathrm{h}} + c_{\mathrm{e}} + c_{\mathrm{t}} + c_{\mathrm{o}} + c_{\mathrm{r}} + c_{\mathrm{v}} \tag{17}$$

Here, c_p is the total cost of actively remanufacturing hot-rolling work rolls; c_l is the cost of laser cladding remanufacturing; c_c is the cost related to machining; c_a is the cost related to heat treatment; c_d is the cost of cleaning and descaling the rolls; c_h is the labor costs; c_e is the cost of equipment depreciation; c_t covers the expenses for inspection and evaluation; c_o is the administrative and office management costs; c_r is the research and development expense; and c_v covers environmental protection costs.

The renewal-reward theory focuses on analyzing the average cost of equipment during its operational lifetime. This theory simplifies the calculation of long-term average equipment costs by computing the ratio of the total cost incurred in a renewal process to the time spent on that renewal process. Using this approach, decisionmakers can more efficiently assess and optimize equipment remanufacturing timing strategies to reduce operational costs.

The expected cost rate for the operation of the hot-rolling work roll at the k-th monitoring point is calculated. During the rolling roll's operating cycle, the primary sources of costs are the online monitoring cost, the cost of active remanufacturing of the hot-rolling work roll, or the cost of scrapping and replacement of the hot-rolling work roll, as calculated in Section 4.2.1. The online monitoring cost is $k \times c_m$. Therefore, at time t, the expected cost from the start of the hot-rolling work roll to the end of its service is as follows:

$$k \times c_{\mathrm{m}} + c_{\mathrm{p}} + (c_{\mathrm{f}} - c_{\mathrm{p}}) \Pr(L_k < s - t_k \mid X_k) \tag{18}$$

where c_m is the cost of a single online monitoring cycle; c_p is the cost of actively remanufacturing the hot-rolling work roll;

c_f is the cost of scrapping and replacing the hot-rolling work roll; and $\Pr(L_k < s - t_k \mid X_k)$ is the failure probability of the hot-rolling work roll.

The expected service duration is as follows:

$$t_k + (s - t_k)(1 - \Pr(L_k < s - t_k \mid X_k)) + \int_0^{s-t_k} l_k f_{L_k|x_k}(l_k \mid x_k) dl_k \quad (19)$$

Combining Equations 4.5 and 4.6, the expected cost rate to proactively remanufacturing hot-rolling work rolls at time t_k is as follows. In summary, at the k-th monitoring point, the proactive remanufacturing timing for hot-rolling work rolls is to minimize the expected cost rate while ensuring reliability at the moment of proactive remanufacturing. The specific expression is as follows:

$$C(s) = \frac{k \times c_m + c_p \times \left(1 - F_{L_k|x_k}(s - t_k)\right) + c_f \times F_{L_k|x_k}(s - t_k)}{t_k + \int_0^{s-t_k} \left(1 - F_{L_k|x_k}(u)\right) du} \quad (20)$$

$$\begin{cases} \min C(s) = \dfrac{k \times c_m + c_p \times \left(1 - F_{L_k|x_k}(s - t_k)\right) + c_f \times F_{L_k|x_k}(s - t_k)}{t_k + \int_0^{s-t_k} \left(1 - F_{L_k|x_k}(u)\right) du} \\ s.t \quad R_{s|t_k}(s - t_k) \geq R_{\min} \\ \qquad s \geq t_k \end{cases} \quad (21)$$

3. Experimental Validation

3.1. Experimental Design and Data Collection

3.1.1. Hot-Rolling Simulation Experiment

To simulate the working conditions of industrial rolling mills, a hot-rolling simulation two-roll test rig (Figure 3) was developed. The test rig mainly consists of a test roll, a load roll, an eddy current detection system, a cooling device, and an induction heating device.

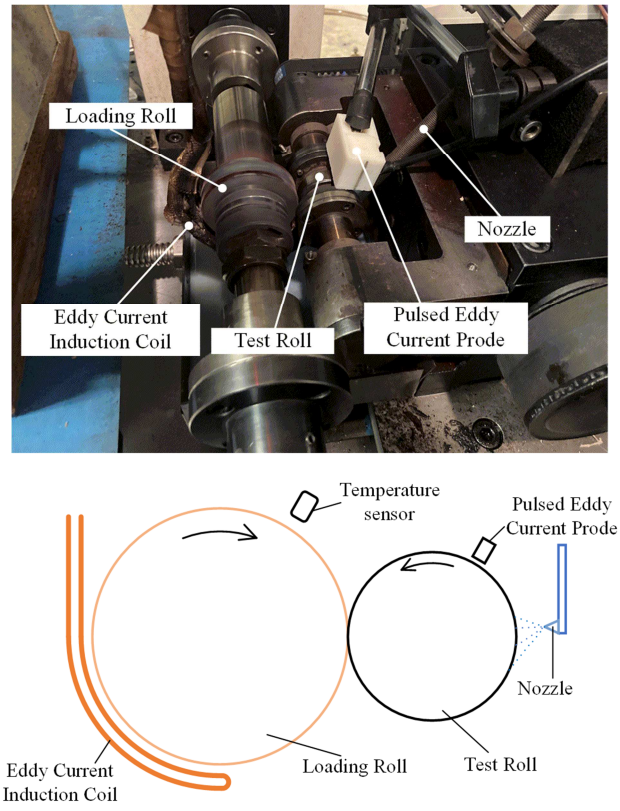

Figure 3. *Hot rolling simulation roll testing device with its sketch.*

The work roll was simulated using the test roll, and the steel strip to be rolled was simulated using the load roll. The test roll and load roll were separately controlled by two servo motors. The rolling force was applied through a set of ball screw servo loading systems, which could exert a maximum load of 6000 N. To heat the load roll to the temperature reached by rolled steel strips in industrial rolling, a high-frequency induction heating device was used. The power of this device is 25 kW, and it can reach temperatures as high as 1200°C within 5 minutes, as monitored by temperature sensors placed above the load roll. The high-frequency induction heater, temperature sensor, and power regulator together form a closed-loop control heating system. The cooling device is similar to those used in actual industrial environments. After the test roll and load roll make contact, a cooling device sprays emulsion coolant at a position 120° be-hind the contact area on the test roll. The emulsion coolant serves both cooling and lubrication purposes. Table 1 shows the specific test parameters.

Table 1. *Hot rolling simulation test conditions.*

Parameters	Value
Test roll revolution/(r/min)	10
Hertzian contact stress/N	750
Loading roll temperature/℃	950
Force/N	2 500
Slippage rate (%)	5
Cycle interval/r	5 000
Number of cycles	23

3.1.2. Sample Preparation

The test roll had a base material made of QT700-2 nodular cast iron. A cladding layer was added to the surface of the nodular cast iron base material. The cladding layer used high-carbon, high-speed steel powder with a particle size of 45–100 μm. The load roll was made of 45 steel. Both test roll base material and load roll blank were made from annealed round bars, and high-precision lathes, grinders, and boring ma-chines were used to machine the outer circumference,

inner bore, keyway, and end face of the rolls. The cladding layer of the test roll was obtained through single-pass clad-ding using an ND-YAG laser for lateral powder feeding. Table 2 shows the cladding parameters.

Table 2. *Melting parameters.*

Parameters	Value
Voltage /V	380
Current /A	210
Average laser power /W	900
Scanning speed /(mm/min)	120
Powder feeding rate /(g/min)	7
Spot diameter /mm/	2
Protective gas flow rate /(L/min)	10

Subsequently, the test roll underwent the following heat treatment process: It was first subjected to a thorough austenitization process at 1050°C, followed by air quenching. Finally, the specimen was subjected to two high-temperature tempering processes at 550°C. Both test roll and load roll were thoroughly cleaned in an ultrasonic cleaning machine using anhydrous ethanol as the cleaning agent to remove surface stains and machining residues.

3.1.3. Roller Degradation Detection and Monitoring

Each revolution of the specimen is equivalent to rolling a 2.513 m-long piece on the precision rolling mill with a roll diameter of 1780 mm. Surface condition monitoring and analysis of the work rolls were conducted every 5000 revolutions. The experiment consisted of three sets, which involved three test rolls in total. Each test roll had eight fixed monitoring points, and the degradation data for the test rolls were obtained by averaging the data from these eight points. The data from the first two sets of experiments were used as the training dataset, and the data from the last set of experiments were used as the test dataset.

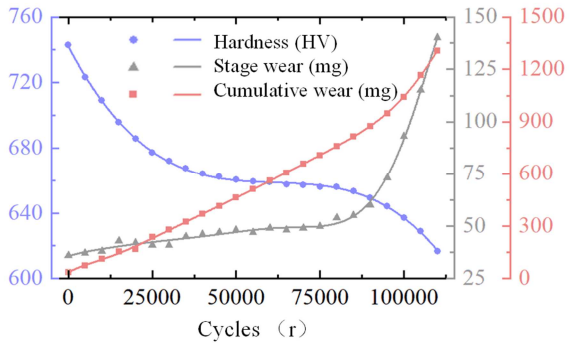

Figure 4. *The changes in roll hardness, wear amount, and wear resistance.*

The surface morphology and microstructure of the test roll were characterized using a ZEISS Gemini 500 scanning electron microscope and an Optika B-500MET/XDS-3MET optical microscope. Hardness measurements were conducted using a microhardness tester. For this study, 16 sets of hardness data were randomly obtained for each test roll in each state cycle, and the average value was taken. The change in roll quality served as a basis for roll wear, and the average wear amount for the test roll was calculated. Roll wear at different stages was quantified as the roll stage wear. Figure 4 illustrates the changes in roll hardness, wear amount, and wear resistance. Torque sensors were installed on the drive shaft, as shown in Figure 5.

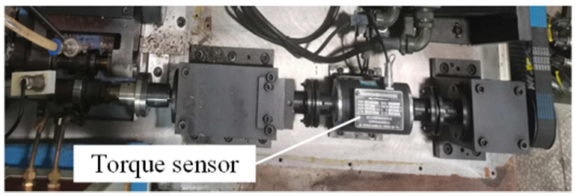

Figure 5. *Torque Sensor Installation Diagram.*

To collect pulsed eddy current signals from the surface of the work roll, a pulsed eddy current detection system was constructed. To ensure that the pulsed eddy current probe could provide sufficient magnetic field energy and effectively receive the eddy current response during the detection process, the optimal design parameters for the probe were determined with the assistance of the electromagnetic simulation module of the COMSOL Multiphysics finite element simulation software. Table 3 lists the parameters of the pulsed eddy current detection system. Figure 6 shows the detected raw pulsed eddy current signals.

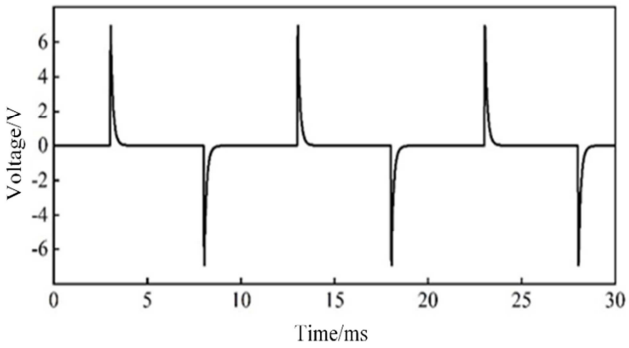

Figure 6. *The detected raw pulsed eddy current signals.*

Table 3. *Pulsed eddy current inspection system parameters.*

Parameters	Value
Core height /mm	14
Core diameter /mm	4
Excitation coil turns	250
Detection coil turns	500
Square wave frequency /Hz	100
Duty cycle (%)	50
Maximum voltage /V	6
Rise time /ms	0.02
Down time /ms	0.02

3.2. Degradation Characterization and Online Feature Extraction

3.2.1. Roller Degradation Characterization

Figure 6 shows the degradation trends of the roll hardness, wear amount, and wear resistance, which were fused into the roll health indicator (HI) using the Beta distribution method. The roll performance is inversely proportional to the HI

value. In this study, the Beta method was used to fuse the primary degradation indicators that affected the roll performance, such as the hardness, wear amount, and wear resistance, to construct a fused HI. This fused HI serves as the basis for evaluating the re-manufacturability of rolls. Shifting the focus to the knee (-onset & -point) enables an earlier detection of accelerated health degradation, leading to more effective predictive maintenance. The Ville inflection detection method is a set of inflection detection methods using the mathematical definition of curvature as the basis for the definition of inflection points, for discrete data, combined with different application scenarios of offline and on-line [20] Taking the figure as an example, point A is the performance degradation inflection point detected using the Ville detection method, which corresponded to a rotation count of 85,000 revolutions. Thus, the roll operated normally in the range of 0–85,000 revolutions, and its performance rapidly degraded after 85,000 revolutions. Therefore, the roll must be re-manufactured before reaching 85,000 revolutions, but the specific timing of remanufacturing should also consider economic benefits.

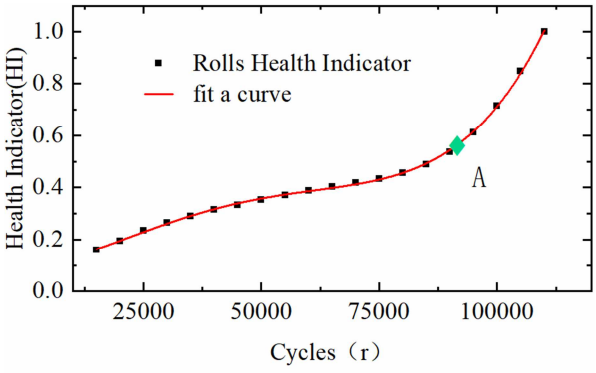

Figure 7. *Degradation trends of HI.*

3.2.2. Online Feature Extraction

The surface friction coefficient obtained through torque sensor monitoring is shown in the table. In the range of 0–10,000 revolutions, the surface friction coefficient first decreased and subsequently increased. This behavior is attributed to the presence of distinct initial machining marks on the roll's surface at zero revolutions (as shown in Figure 8).

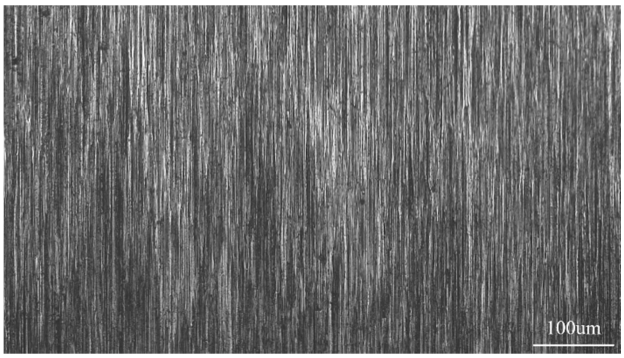

(a) 0 r

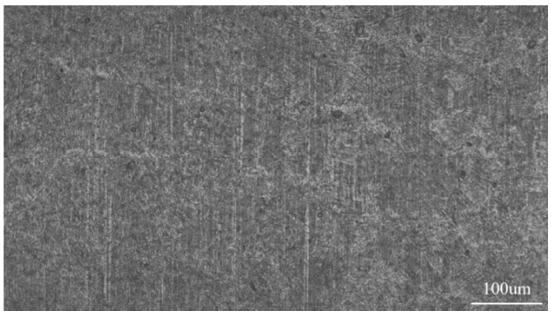

(b) 10000 r

Figure 8. *0-10000 r Roll surface initial machining marks change: (a) 0 r; (b) 10000 r.*

The existence of these initial machining marks indicates that the initial surface quality of the roll has not reached its optimal state. After the roll and rolled material had been running for 10,000 revolutions, the machining marks on the roll's surface disappeared, which reduced the measured surface friction coefficient "f" from 0.20 to 0.17, as indicated in Table 4.

Table 4. *Variation of friction coefficient on test roll surface7.*

Revolutions /r	Friction coefficient
10 000	0.170±0.001
20 000	0.162±0.001
30 000	0.160±0.001
40 000	0.161±0.002
50 000	0.164±0.001
60 000	0.166±0.001
70 000	0.170±0.002
80 000	0.175±0.002
90 000	0.180±0.002
100 000	0.192±0.003
110 000	0.220±0.003

Therefore, the surface friction coefficient was not in its optimal state at the initial stage, and it reached its optimal state after 10,000 revolutions. The high surface friction coefficient in the early stage is related to the initial machining method. Due to this reason and the impossibility of the roll remanufacturing point occurring in the early stage, in this study, we consider the selection of the roll remanufacturing point and model training starting from 15,000 revolutions to eliminate the influence of the initial processing method on the model accuracy.

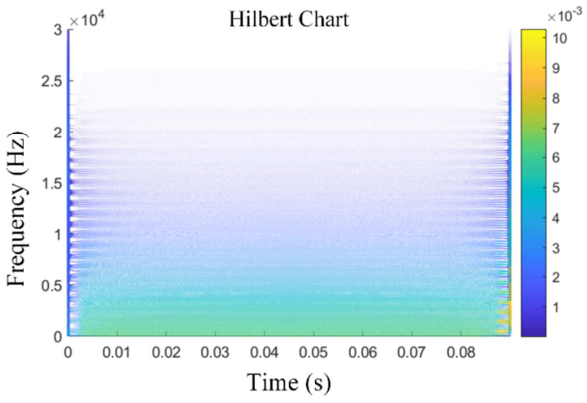

Figure 9. *Hilbert spectrum.*

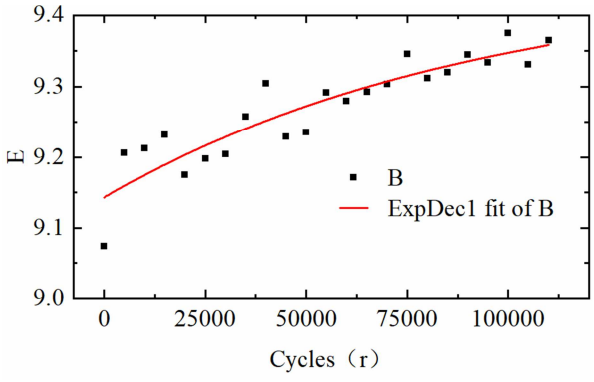

Figure 10. *The change of cumulative energy.*

Figure 9 shows the Hilbert spectrum of the original eddy current signal after the VMD-Hilbert transformation, and Figure 10 shows the cumulative energy.

3.3. Comparative Analysis of Models

To verify the superiority of the MLP model in predicting the degradation state of hot-rolling work rolls, multiple linear regression and support vector machine (SVM) regression using multi-sensor signals were compared for their prediction of the degradation state of hot-rolling work rolls. Figure 11 shows the results. A comparison of Figure 11(a)–(c) shows that the MLP model has the best predictive performance com-pared with the actual performance degradation process of the rolls. The SVM model has better predictive performance than the multiple linear regression model. Figure 11(b) shows that the SVM model exhibits good accuracy in the early stage of prediction, but its effectiveness in predicting the rapid degradation process in the later stage is unsatisfactory. Meanwhile, the multiple linear regression model shows a significant disparity from the actual values throughout the entire degradation process.

From Figure 11, the selected method in this study exhibits smaller errors in predicting the degradation of the roll performance, which validates the superiority of the MLP model in predicting the roll performance degradation. Additionally, the predictive performance of the three methods was qualitatively analyzed, as presented in Table 5.

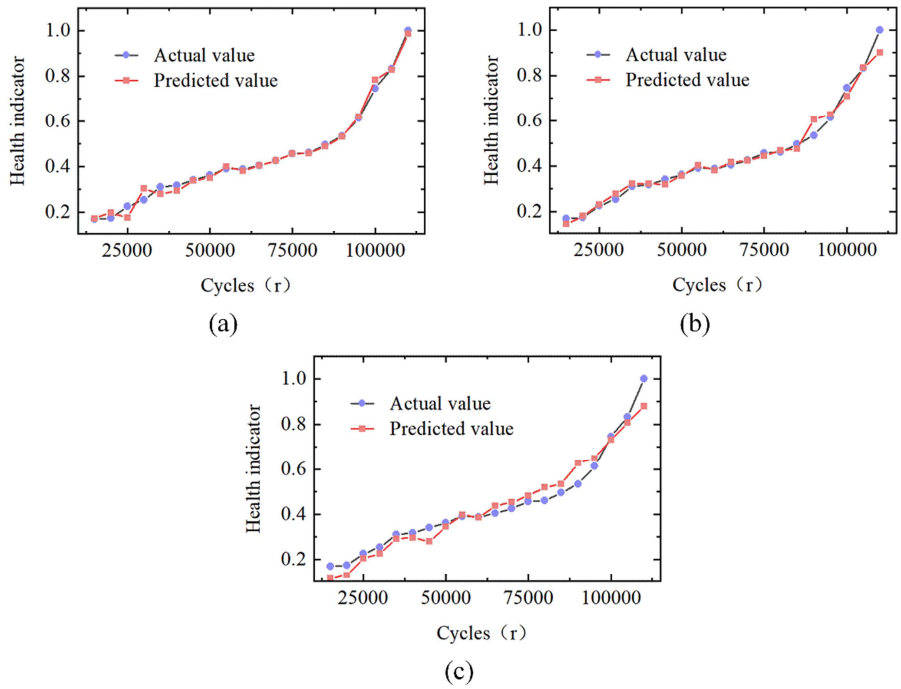

Figure 11. *Prediction results of roll degradation by three models: (a) MLP model; (b) SVM; (c) Multiple linear regression.*

Table 5. *Performance comparison of different algorithms for the roll degradation prediction.*

	MLP	Multiple linear regression model	SVM
MAE	0.014244484	0.038241054	0.019873497
RMSE	0.020934754	0.027139403	0.022376578

The MLP model predicts the roll degradation status with small MAE and RMSE, which are 0.01424 and 0.2093, respectively. When the multiple linear regression model and SVM model are used to predict roll degradation, they yield larger errors than the proposed method, and both MAE and RMSE values are higher than the MLP model prediction error. Therefore, the research findings suggest that this method has made some progress in exploring the underlying patterns between the extracted online features and the roll degradation.

Now, based on the actual production and operation of the third-stand hot-rolling work rolls in a precision rolling mill unit of a certain factory, the hot-rolling work roll scrapping and replacement cost and active remanufacturing cost can be

reasonably determined. Tables 6 and 7 show the specific cost breakdown.

Considering various factors, the hot-rolling work roll scrapping and replacement cost cf is 160,000 yuan, and the hot-rolling work roll active remanufacturing cost cp is 55,000 yuan. In the hot-rolling work roll active remanufacturing timing prediction model, it is also necessary to set the monitoring interval and cost required for each monitoring. To match the experimental process, it is set that for every 5000 revolutions of the hot-rolling work roll, surface monitoring is performed once, and the cost of each monitoring is 1000 yuan, i.e., cm = 1000 yuan.

Table 6. *Work roll scrapping replacement cost in hot rolling.*

Item	Cost/$	Item	Cost/$
Purchase cost of new roller c_n	150000	Depreciation cost of related equipment c_e	2000
Disposal cost of used work roll c_w	5000	Testing and evaluation cost c_t	1000
Labor Costs c_h	1500	Office Administration Costs c_o	500

Table 7. *Active remanufacturing cost of work roll in hot rolling.*

Item	Cost/$	Item	Cost/$
Laser cladding remanufacturing cost c_l	36000	Depreciation cost of related equipment c_e	2500
Machining Related Costs c_c	4000	Testing and Evaluation Costs c_t	2000
Heat treatment related expenses c_a	2000	Office administration expenses c_o	1000
Roll cleaning and descaling cost c_d	1500	R&D cost c_r	2000
Labor Costs c_h	3000	Environmental Protection Costs c_y	1000

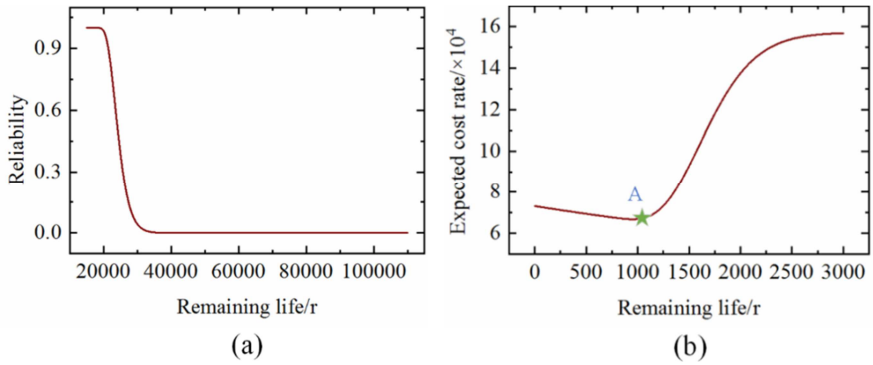

Figure 12. *Reliability Curve and Expected Cost Rate Curve at 80,000r for Test Roll No. 3(a) Reliability Curve; (b) Expected Cost Rate Curve.*

Based on the Wiener method to calculate the reliability at each monitoring point, combined with the update-reward theory to give the optimal remanufacturing time of the rolls, Figure 12 shows the reliability curve of the rolls at 80,000 r and the expected cost rate curve, in which the optimal remanufacturing point is 81105r, the lowest expected cost rate of 6.687 ¥/r, shown at point A in Figure 12(b).

4. Conclusion

This study presents a method for online decision-making regarding the prediction of the degradation status and proactive remanufacturing timing of hot-rolling work rolls, which combines a multi-sensor multi-feature fusion with an MLP model while considering economic factors. The following conclusions can be drawn from this study:

(1) By collecting degradation-related quantities during the hot-rolling simulation experiment and fusing them through a Beta distribution, a degradation indicator for rolling rolls was constructed. This indicator comprehensively characterizes the degradation status of the rolls to avoid the one-sided representation of the roll state caused by a single degradation quantity.

(2) The torque and pulsed eddy current signals were collected during the roll degradation process. By analyzing the original signals, friction coefficients were extracted with pulse eddy current time-frequency domain features. These online features were combined as input parameters for the MLP model. This approach avoids the influence of redundant information on MLP model training and reduces the training time, which enhances the training accuracy of the model. The established MLP model was com-pared with multiple linear regression and SVM models, which validates the superiority and advancement of the MLP model in roll degradation prediction and enables the online monitoring of roll performance degradation.

(3) Combining the MLP model with the Wiener and updating-reward theories, this study successfully monitored the roll degradation status online, predicted it, and determined the economically optimal point for roll remanufacturing while satisfying the performance requirements.

The proposed online decision-making method to predict the degradation status and determine the optimal remanufacturing time of hot-rolling work rolls in this study has achieved comprehensive assessment and real-time monitoring of the roll status. This approach significantly

reduces the uncertainty of the roll retirement time and performance and provides important implications for real-time monitoring during roll operation and subsequent remanufacturing efforts. It holds great promise for further development in the field of roll status monitoring and remanufacturing. In future works, we plan to expand the types of features and the original signals.

Funding

National Natural Science Foundation of China, grant number UID: 52275483

Conflicts of Interest

The authors declare no conflicts of interest.

References

[1] G. Singh and P. K. Singh, "Effect of process parameters on roll separating force, driving torque and end crop length during grooved hot rolling of SAE 1020 steel," *Journal of Manufacturing Processes*, vol. 79, pp. 1003–1016, Jul. 2022, doi: 10.1016/j.jmapro.2022.05.015.

[2] K. Hu, Y. Xia, F. Zhu, and N. Noda, "Evaluation of Thermal Breakage in Bimetallic Work Roll Considering Heat Treated Residual Stress Combined with Thermal Stress during Hot Rolling," *steel research int.*, vol. 89, no. 4, p. 1700368, Apr. 2018, doi: 10.1002/srin.201700368.

[3] C. Wei, S. Song, and Z. Zhang, "Evaluation of elastic-plastic deformation in HSS work roll under coupling of residual stress thermal stress and contact stress during hot rolling," *Materials Today Communications*, vol. 33, p. 104613, Dec. 2022, doi: 10.1016/j.mtcomm.2022.104613.

[4] Q. Dong, Z. Wang, Y. He, L. Zhang, F. Shang, and Z. Li, "The effect of shifting modes on work roll wear in strip steel hot rolling process," *Ironmaking & Steelmaking*, vol. 50, no. 1, pp. 67–74, Jan. 2023, doi: 10.1080/03019233.2022.2083929.

[5] F. Weidlich, A. P. V. Braga, L. G. D. B. Da Silva Lima, M. B. Júnior, and R. M. Souza, "The influence of rolling mill process parameters on roll thermal fatigue," *Int J Adv Manuf Technol*, vol. 102, no. 5–8, pp. 2159–2171, Jun. 2019, doi: 10.1007/s00170-019-03293-1.

[6] S. Wu, W. Xing, Y. Liu, and Y. Shao, "Research on dynamic characteristics and identification method of local defect on the roll surface," *Engineering Failure Analysis*, vol. 121, p. 105063, Mar. 2021, doi: 10.1016/j.engfailanal.2020.105063.

[7] C. Li, H. Yu, G. Deng, X. Liu, and G. Wang, "Numerical Simulation of Temperature Field and Thermal Stress Field of Work Roll During Hot Strip Rolling," *J. Iron Steel Res. Int.*, vol. 14, no. 5, pp. 18–21, May 2007, doi: 10.1016/S1006-706X(07)60067-3.

[8] N. F. Garza-Montes-de-Oca, R. Colás, and W. M. Rainforth, "On the damage of a work roll grade high speed steel by thermal cycling," *Engineering Failure Analysis*, vol. 18, no. 6, pp. 1576–1583, Sep. 2011, doi: 10.1016/j.engfailanal.2011.06.001.

[9] L. Xu, W. Song, S. Ma, Y. Zhou, K. Pan, and S. Wei, "Effect of slippage rate on frictional wear behaviors of high-speed steel with dual-scale tungsten carbides (M6C) under high-pressure sliding-rolling condition," *Tribology International*, vol. 154, p. 106719, Feb. 2021, doi: 10.1016/j.triboint.2020.106719.

[10] G. Y. Deng *et al.*, "Theoretical and experimental investigation of thermal and oxidation behaviours of a high speed steel work roll during hot rolling," *International Journal of Mechanical Sciences*, vol. 131–132, pp. 811–826, Oct. 2017, doi: 10.1016/j.ijmecsci.2017.08.024.

[11] G. Y. Deng *et al.*, "Evolution of microstructure, temperature and stress in a high speed steel work roll during hot rolling: Experiment and modelling," *Journal of Materials Processing Technology*, vol. 240, pp. 200–208, Feb. 2017, doi: 10.1016/j.jmatprotec.2016.09.025.

[12] C. G. Sun, S. M. Hwang, C. S. Yun, and J. S. Chung, "Investigation of thermomechanical behavior of a work roll and of roll life in hot strip rolling," *Metall Mater Trans A*, vol. 29, no. 9, pp. 2407–2424, Sep. 1998, doi: 10.1007/s11661-998-0117-y.

[13] L. Gan, L. Li, and H. Huang, "Digital Twin-Driven Sheet Metal Forming: Modeling and Application for Stamping Considering Mold Wear," *Journal of Manufacturing Science and Engineering*, vol. 144, no. 121003, Jul. 2022, doi: 10.1115/1.4054902.

[14] L. Gan, H. Huang, L. Li, W. Xiong, and Z. Liu, "IoT-enabled energy efficiency monitoring and analysis method for energy saving in sheet metal forming workshop," *J. Cent. South Univ.*, vol. 29, no. 1, pp. 239–258, Jan. 2022, doi: 10.1007/s11771-022-4933-9.

[15] H. B. Lim, H. I. Yang, and C. W. Kim, "Analysis of the roll hunting force due to hardness in a hot rolling process," *J Mech Sci Technol*, vol. 33, no. 8, pp. 3783–3793, Aug. 2019, doi: 10.1007/s12206-019-0721-3.

[16] H. Xu and H. Huang, "CNN architecture-based hybrid fusion model for in-situ monitoring to fabricate metal matrix composite by laser melt injection," *J Intell Manuf*, Sep. 2023, doi: 10.1007/s10845-023-02207-z.

[17] F. Delaunois, V. I. Stanciu, A. Megret, and M. Sinnaeve, "Oxidation and wear behavior of high-speed steel and semi-high-speed steel used in hot strip mill," *Int J Adv Manuf Technol*, vol. 119, no. 1, pp. 677–689, Mar. 2022, doi: 10.1007/s00170-021-08031-0.

[18] C. Bataille, E. Luc, M. Bigerelle, R. Deltombe, and M. Dubar, "Rolls wear characterization in hot rolling process," *Tribology International*, vol. 100, pp. 328–337, Aug. 2016, doi: 10.1016/j.triboint.2016.03.012.

[19] M. Marani, M. Zeinali, V. Songmene, and C. K. Mechefske, "Tool wear prediction in high-speed turning of a steel alloy using long short-term memory modelling," *Measurement*, vol. 177, p. 109329, Jun. 2021, doi: 10.1016/j.measurement.2021.109329.

[20] P. Fermín-Cueto *et al.*, "Identification and machine learning prediction of knee-point and knee-onset in capacity degradation curves of lithium-ion cells," *Energy and AI*, vol. 1, p. 100006, Aug. 2020, doi: 10.1016/j.egyai.2020.100006.